

Article

Stimulating Nitrogen Biokinetics with the Addition of Hydrogen Peroxide to Secondary Effluent Biofiltration

Liron Friedman ^{1,2,3}, Hadas Mamane ², Kartik Chandran ³, Martin Jekel ⁴, Haim Cikurel ⁵, Uwe Hübner ⁶, Michael Elgart ⁷, Shlomi Dagan ⁷, Jorge Santo-Domingo ⁸ and Dror Avisar ^{1,*}

¹ The Water Research Center, School of Earth Sciences, Faculty of Exact Sciences, Tel Aviv University, Tel Aviv 69978, Israel; lirfri@gmail.com

² School of Mechanical Engineering, Faculty of Engineering, Tel Aviv University, Tel Aviv 69978, Israel; hadasmg@tauex.tau.ac.il

³ Department of Earth and Environmental Engineering, Columbia University, New York, NY 4711, USA; kc2288@columbia.edu

⁴ Department of Water Quality Control, Technical University of Berlin, 10623 Berlin, Germany; martin.jekel@tu-berlin.de

⁵ Environmental Services, consultant, Bat-Yam 59555, Israel; chikurel@netvision.net.il

⁶ Urban Water Systems Engineering, Technical University of Munich, 85748 Garching, Germany; u.huebner@tum.de

⁷ Weizmann Institute of Science, Molecular cell biology, Rehovot 76100, Israel; Elgart@gmail.com (M.E.); Shlomi.dagi@gmail.com (S.D.)

⁸ US Environmental Protection Agency; National Risk Management Research Laboratory, Cincinnati, OH 45268, USA; santodomingo.jorge@epa.gov

* Correspondence: droravi@tauex.tau.ac.il; Tel.: +972-3-6405534

Received: 22 December 2019; Accepted: 20 January 2020; Published: 1 February 2020



Abstract: Tertiary wastewater treatment could provide a reliable source of water for reuse. Amongst these types of wastewater treatment, deep-bed filtration of secondary effluents can effectively remove particles and organic matter; however, NH_4^+ and NO_2^- are not easily removed. This study examined the feasibility of stimulating microbial activity using hydrogen peroxide (H_2O_2) as a bio-specific and clean oxygen source that leaves no residuals in the water and is advantageous upon aeration due to the solubility limitations of the oxygen. The performance of a pilot bio-filtration system at a filtration velocity of 5–6 m/h, was enhanced by the addition of H_2O_2 for particle, organic matter, NH_4^+ , and NO_2^- removal. Hydrogen peroxide provided the oxygen demand for full nitrification. As a result, influent concentrations of 4.2 ± 2.5 mg/L N- NH_4^+ and 0.65 ± 0.4 mg/L N- NO_2^- were removed during the short hydraulic residence time (HRT). In comparison, filtration without H_2O_2 addition only removed up to 0.6 mg/L N- NH_4^+ and almost no N- NO_2^- . A DNA metagenome analysis of the functional genes of the media biomass reflected a significant potential for simultaneous nitrification and denitrification activity. It is hypothesized that the low biodegradability of the organic carbon and H_2O_2 addition stimulated oxygen utilization in favor of nitrification, followed by the enhancement of anoxic activity.

Keywords: hydrogen peroxide; high-rate biofiltration; nitrification; denitrification

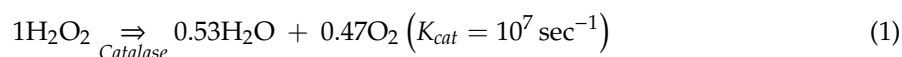
1. Introduction

The tertiary and advanced treatment of wastewater improves water quality, enabling us to meet environmental concerns but also find a potential source of water for reuse [1,2]. The filtration of coagulated–flocculated effluent via high-rate deep-bed filters (velocities between 5 and 20 m/h) is widely

used for tertiary wastewater treatment [3]. The removal mostly combines particles and some dissolved organic matter (15%–20%) [4]. A hybrid process of filtration and bioactivity, termed biofiltration, allows significant nutrient and organic matter removal in addition to particle filtration [5–7].

Molecular methods provide better insight into the processes that are essential for optimal system design. Recent research on the treatment of secondary effluent or groundwater, as sand-filtration and AOP processes, such as UV/H₂O₂, made use of advanced methods as metagenomics, metaproteomics or metatranscriptomics, to analyze the structure of the community attached to the media and determine the related metabolism [8–12].

In biological wastewater systems, dissolved oxygen (DO) is a key parameter in system performance and plays an important role in biotransformation pathways and rates [13,14]. The competition for oxygen among ammonia-oxidizing bacteria (AOB), nitrite-oxidizing bacteria (NOB), and ordinary heterotrophic organisms (OHO) results in oxygen depletion; this, in turn, increases the potential for anoxic (carbon oxidation through reduction of NO₂[−] or NO₃[−]) pathways, such as full or partial denitrification, depending on substrate availability and biodegradability [15–18]. Compared to suspended growth systems, nitrification activity can increase significantly in attached biomass systems when oxygen is more available [19]. DO concentration in the attached biomass is limited by the temperature of the solute (~8 mg/L at 25 °C) and decreases along the biofilm depth, resulting in increased denitrification rates [20,21]. To overcome these limitations, a few studies have examined the use of 100% pure oxygen or hydrogen peroxide (hereafter H₂O₂) degradation (Equation (1)) in attached-biomass systems [22–25].



H₂O₂ degradation by the enzyme catalase. Stoichiometry is by weight (g); K_{cat} —catalytic reaction rate [26].

Catalase is a significant component of the cell defense mechanism against oxidative stress, it scavenges two molecules of H₂O₂ into water and molecular oxygen in one of the highest documented enzyme reaction rates [27,28].

H₂O₂ has advantages as a supplemental oxygen source, namely, high solubility in aqueous solution and an improved mass transfer of dissolved H₂O₂ (liquid–liquid) into the permeable biofilm compared to oxygen that depends also on the oxygen–water transfer into the liquid phase. In addition, rapid H₂O₂ degradation is bacterium-specific and leaves no persistent residual traces in the water. The disinfection characteristics of H₂O₂ could limit microbial-based reactors, which depend on concentration and time (C × t). Significantly tolerant degradation rates and oxygen utilization have been observed in biofilms, in comparison to suspended bacteria, in addition to changes in microbial community structure [29–33]. However, the application of H₂O₂ as a supplemental oxygen source via high-rate media filtration for NH₄⁺ removal at a short hydraulic residence time (HRT) has never been examined. In this study, we demonstrate the impact of adding H₂O₂ as a supplemental oxygen source on the operational efficiency of a secondary effluent filtration system with biologically active media. The setup design was aimed at combining the removal of particles, NH₄⁺, and, especially, NO₂[−] to reduce ozone demand for a subsequent ozonation treatment (detailed in Zucker et al., [34]). In short, the biofilter was part of a multistep pretreatment unit prior to ozonation to allow better soil aquifer treatment (SAT) performance by reducing particle clogging and minimizing oxygen demand during infiltration in the upper-layer SAT. The specific goals of this study were to examine whether significant biotransformation can be achieved with high-rate (relative to standard biofiltration) filtration conditions and H₂O₂ addition.

2. Experiments

2.1. Pretreatment System Setup

The biofilter system was operated in direct-filtration at the pilot site of the Shafdan wastewater treatment plant (WWTP), operated by Mekorot. The biofilter system, detailed in Figure 1, was part of the multistage setup specified herein:

- Feed flow was $6 \text{ m}^3/\text{h}$ ($144 \text{ m}^3/\text{day}$) of the secondary effluent from the WWTP (Figure 1a) following a $500\text{-}\mu\text{m}$ wire-mesh filtration (Figure 1b) to remove coarse particles.
- Coagulation/flocculation was carried out by injecting polyaluminum chloride (PACl, $18\% \text{ Al}_2\text{O}_3$) by peristaltic pump (Figure 1c) to achieve a final concentration of $\sim 2.7\text{--}3.6 \text{ mg/L}$ as PACl. Flocculation was performed in a modified flocculator, which consisted of a pressure filter (Figure 1d) with $\sim 15 \text{ min}$ hydraulic retention time (HRT). PACl was chosen for this study as it has been shown to be preferable for flocculation and is widely used [35,36].
- Following flocculation, H_2O_2 was added (10%) to the inlet of the high-rate biofilter (Figure 1f) using a peristaltic pump (Figure 1e). The final concentration of 27 mg/L was achieved to provide a surplus of DO for full nitrification of $3.5 \text{ mg/L-N NH}_4^+$ and $0.5 \text{ mg/L-N NO}_2^-$. The biofilter tank had a surface area of 1.13 m^2 , 1.2 m diameter, 1.1 m^3 media volume, and 36% free headspace (additional characteristics are specified in Zucker et al., [34]).

During the adjustment period with stepwise H_2O_2 addition, an average measured concentration of $4.29 \pm 0.56 \text{ mg/L}$ DO at the outlet of the filter was obtained with the addition of $\sim 27 \text{ mg/L}$ H_2O_2 . The theoretical calculation of oxygen mass balance is provided in Appendix A.1. During the research period, the loads of NH_4^+ in the secondary effluent increased due to changes in the process of the plant, which enabled investigating the system performance for NH_4^+ oxidation and N removal under higher NH_4^+ loads and O_2 limitation.

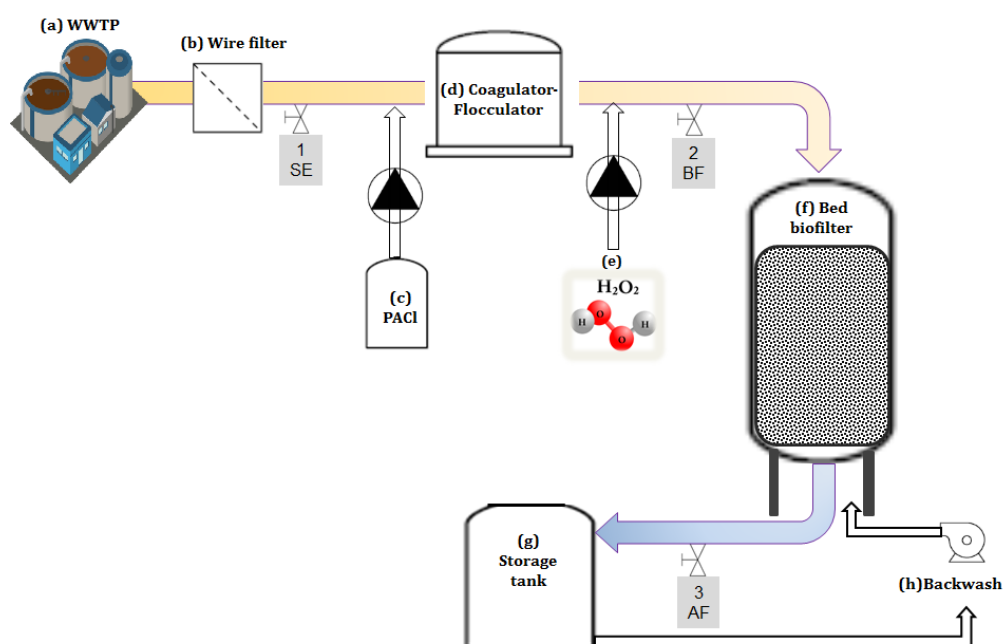


Figure 1. Diagram of biofiltration setup. (a) Secondary effluent from the Shafdan wastewater Table 500 m, (b) wire filter, (c) the addition of polyaluminum chloride (PACl) from a tank, (d) the coagulator–flocculator tank, (e) the addition of H_2O_2 , (f) the bed biofilter, (g) the storage tank, and (h) the backwash pump. Sampling points were located (1) right after the wire-mesh filter, termed the secondary effluent (SE), (2) after flocculation–coagulation and H_2O_2 addition, but before the biofilter (BF) and (3) after the biofilter (AF).

2.2. System Specification and Operational Parameters

The biofiltration was operated with a modified active media filter, operated in downflow mode, with a filtration velocity of $5\text{--}6 \text{ m/h}$ ($\sim 5 \text{ min}$ hydraulic residence time (HRT, the low range of high-rate filtration) and a backwash cycle every 12 h. The filtered effluent water was stored in a 10-m^3 tank (Figure 1g) and was used for backwash. Adjustments were performed to avoid the clogging of the filter while maintaining a steady and active biomass to avoid the detachment of biofilm from the media

(Appendix A.2). The microbial community of the biomass was indigenous and developed over time by feeding the biofilter with the secondary effluent. It was assumed that the accumulation and growth of viable bacteria in the filter, most of which were fixed to the media, was the basis for the bacterial activity [6,37–39].

2.3. Solute Sampling and Analyses

After two months of system operation without H₂O₂ addition, samples were further taken over for a period of four months with stable performance. Stabilization after H₂O₂ addition took also about two months and then a sampling campaign was conducted every 2–4 weeks for over two years. At every sampling campaign, samples were collected 6–7 h after the start of the morning filtration cycle (middle of the cycle) from sampling faucet located past the mesh filter, named the secondary effluent (SE), before the biofilter (BF) and after the biofilter (AF). An analysis of water characteristics was conducted at the Shafdan WWTP laboratory specified in the Appendix A.3.

2.4. Particle Sampling and Analysis

Effluent particles and aggregates were analyzed by Micro Flow Imaging (MFI) technology (DPA 4100, Protein Simple Inc., Ottawa, ON, Canada). This apparatus employs a digital camera with an illumination and magnification system to capture in-situ images of suspended particles in a flowing sample. A detailed description of this analysis is published elsewhere [32,36]. An analysis was conducted on particles of between ~2 and 400 µm.

2.5. Media Sampling and Metagenome Analysis

A metagenome analysis was conducted to investigate the functional potential of the microbial community in the media. In the middle of the operation cycle (6 h), the biofilter was emptied and a sample of 50 g anthracite media was taken from a 40-cm depth, thoroughly mixed for homogenization, and immediately stored in dry ice. Sampling was conducted a few days after the sampling campaign designated in star in Figure A1 in the Appendix A. DNA from the media was extracted using an Exgene Soil DNA Kit. The whole-genome (shotgun) libraries were prepared using the TruSeq DNA PCR-Free HT Library Preparation Kit (Illumina, San Diego, CA, USA) and were sequenced using an Illumina MiSeq benchtop sequencer with a target fragment length of 250 bp. After the removal of adapters and low-quality reads, ~8.2 M reads were left with an average length of 225 base pairs. (Appendix A Figure A2). High-quality reads were mapped to N-cycle related genes using BWA [40]. The potential for dominant biotransformation of the microbial community was deduced from the relative abundance of specific functional genes. The genes for nitrification (*amoA*, *nxrB*, *cyt c*), denitrification (*narG*, *nirK*, *nirS*, *norB*, *nosZ*), and other various metabolic pathways, such as methane (*pmoA*), hydrogen sulfide (*drseFH*), and hydrogen (HiFe) oxidation were analyzed and compared on a log scale [9]. The gene catalog was extracted from NCBI's nucleotide database. Genes aligning to the reads were sorted according to their respective identified organisms, which varied between 6%–19% among all the reads related to each gene (Figure A2 in the Appendix A).

3. Results

The goal of this study was to design a biofilter with short HRT to support nitrification activity, by surplus oxygen, for the removal of NO₂⁻ and NH₄⁺. The system showed a significant removal of NO₂⁻ and NH₄⁺ when H₂O₂ was added in comparison to the control. The biofilter was optimized in the matter of H₂O₂ addition and evaluated as a single step in an integrated treatment with the ultimate goal to produce a stream with lower oxygen demand for following SAT or non-potable reuse purposes.

3.1. Particle Distribution

To determine biofilter performance in removing particles as a function of equivalent circular diameter (ECD), and the particles' size and the size distribution in the secondary effluent, a dynamic

image analysis was made. The particle-size distribution (PSD) of secondary effluents based on 13 campaigns is presented in Figure A1 in the Appendix A, taken at the SE sampling point. In general, the PSD was similar in comparison to the high variation in total particle number. Almost all (99%) of the particles were analyzed (<50 μm), with the highest variation in the fraction with ECD = 2–3 μm . The total particle removal performance was found to be highly efficient ($95 \pm 2\%$) for all sampling campaigns. No difference was observed in particle removal without H_2O_2 . A typical PSD analysis of the secondary effluent after 500 μm , post flocculation and after the biofilter, is presented in Figure A1 in the Appendix A. Flocculation before biofiltration increased particle counts due to the flocculation of the macromolecules and colloid particles (<2 μm), which were not analyzed. As expected, particle concentration decreased dramatically after biofiltration for all ECDs.

3.2. H_2O_2 Decomposition

The concentration of DO before filtration varied between 3–5 mg/L. No H_2O_2 was detected at the inlet or outlet during an operation without H_2O_2 addition, while the DO values at the outlet were <1 mg/L, which clearly indicated maximum oxygen utilization and reflected anoxic conditions [20]. The preliminary lab-bench experiments revealed no decomposition of H_2O_2 when mixed with effluents within the interval of the HRT (20 min), as also documented by Lakretz et al. [32]. When H_2O_2 was added, the measured H_2O_2 concentration at the inlet was 27 ± 2 mg/L, and <1 mg/L at the outlet, which affirms full H_2O_2 degradation. Furthermore, DO values after filtration were similar or slightly higher than before filtration. Thus, we conclude that H_2O_2 decomposition in the system occurs almost solely via bacterial activity and functions as a source of available oxygen.

3.3. Reference Measurements—No Addition of H_2O_2

Sampling campaigns were conducted without the addition of H_2O_2 as a reference: DO values at the outlet were <1 mg/L, which reflects maximum oxygen utilization and anaerobic conditions inside the reactor [20]. The dissolved organic carbon (DOC)- and chemical oxygen demand (COD)-removal rates were similar ($13\% \pm 0.3\%$, and $11\% \pm 2\%$, respectively) and were mainly caused by flocculation/filtration. Data were insufficient for the ultra violet absorption (UVA) measurements. The average NH_4^+ , NO_2^- and NO_3^- concentrations at the BF sampling point were 3.1 ± 0.60 mg/L-N, 0.37 ± 0.07 mg/L-N, and 0.34 ± 0.05 mg/L-N, respectively. While NH_4^+ removal was constant at 0.6 ± 0.08 mg/L-N, NO_2^- removal was not constant, and in some samples no removal of NO_2^- was observed. The average increase in NO_3^- concentration was 0.73 ± 0.21 mg/L-N. The calculated nitrogen loss was fairly low and did not exceed $4 \pm 1\%$, which suggests removal by filtration rather than via denitrification.

3.4. Organic Carbon Removal with H_2O_2 Addition

The biofilter removal rates of DOC and UVA were stable at $22\% \pm 5\%$ and $20\% \pm 3\%$, respectively, regardless of the variation in DOC (10.4 ± 1.4 mg/L) and UVA (217 ± 13 m^{-1}) at the inlet. Without H_2O_2 , the ΔDOC , ΔUVA_{254} and ΔCOD was 1.6 ± 0.4 mg/L, 7 ± 1 m^{-1} and 3.3 ± 1 mg/L, respectively. With addition of H_2O_2 , the ΔDOC , ΔUVA_{254} and ΔCOD increased to 2.3 ± 0.7 mg/L, 44 ± 7 m^{-1} and 14.6 ± 4 mg/L, respectively, indicating additional organic carbon utilization by bacteria (Appendix A Figure A5: concentrations and the removal of DOC and UVA_{254} over sampling campaigns before the biofilter and after the biofilter). The oxygen utilization, in favor of nitrification rather than carbon oxidation, reflects the low biodegradability of organic matter, which is typical for effluent post-secondary treatment with flocculation–filtration removal [41–44]. This is also supported by no removal of most trace organic compounds in the biofilter, besides Acesulfame and Iopromide that were removed by 60% and 30%, respectively [34]. These results show that the biofilter was efficient and robust at removing particles, DOC, and UVA.

3.5. NH_4^+ and NO_3^- Transformation, Variation, and Nitrogen Mass Balance

To better illustrate the potential nitrogen transformations in the biofilter due to H_2O_2 addition, and especially the NH_4^+ removal (mg/L-N) ability of the system, the parameters at all the figures were sorted

by NH_4^+ concentrations at the inlet (BF) sampling point, as illustrated in Figure 2. It can be clearly observed that the concentration of NO_3^- that increased at the outlet of the biofilter is in parallel to the decrease in NH_4^+ concentration (Figure 2). Full NH_4^+ removal with H_2O_2 addition was obtained when the BF concentration was lower than 4 mg/L-N, whereas above 4 mg/L-N residual NH_4^+ was detected at the AF sampling point. The average NO_2^- concentration of 0.64 ± 0.4 mg/L-N was fully removed after the biofilter (AF) for all samples (Supporting data Figure A6: removal of NO_2^-), indicating rapid NO_2^- oxidation to NO_3^- (nitrification). Thus, H_2O_2 addition enabled a significantly higher nitrification rate. Given that the nitrification rate in the biofilter was stable and was solely dependent on H_2O_2 addition, regardless of particle numbers and removal, it is suggested that most of the microbial activity occurred in the biomass attached to the media, perhaps independent of the filtration cake and its size. The ammonium oxidation rate (AOR) (the ratio of formed NO_3^- to the transformed NH_4^+ and NO_2^-), is calculated according to Equation (2) and shown for all sampling points

$$\text{AOR} = - \frac{\Delta[\text{NO}_3^- - \text{N}]}{\{\Delta[\text{NH}_4^+ - \text{N}] + \Delta[\text{NO}_2^- - \text{N}]\}} \quad (2)$$

ONT = Ammonification, organic nitrogen transformed to NH_4^+

Nit = Nitrification

NX = Anoxic/AMX (anaerobic ammonia oxidation) nitrogen transformation to dinitrogen

Inorganic nitrogen balance rate to indicate dominant pathway:

When $\text{AOR} > 100\%$, $\text{ONT} + \text{Nit} \gg \text{NX}$

When $\text{AOR} < 100\%$, significant NX

When $\text{AOR} \approx 100\%$, $\text{Nit} \gg \text{ONT}, \text{NX}$

In most samples, AOR revealed values of less than 100% (Figure 2, green dashed line), indicating the loss of ammoniacal nitrogen as dinitrogen, which will be further detailed.

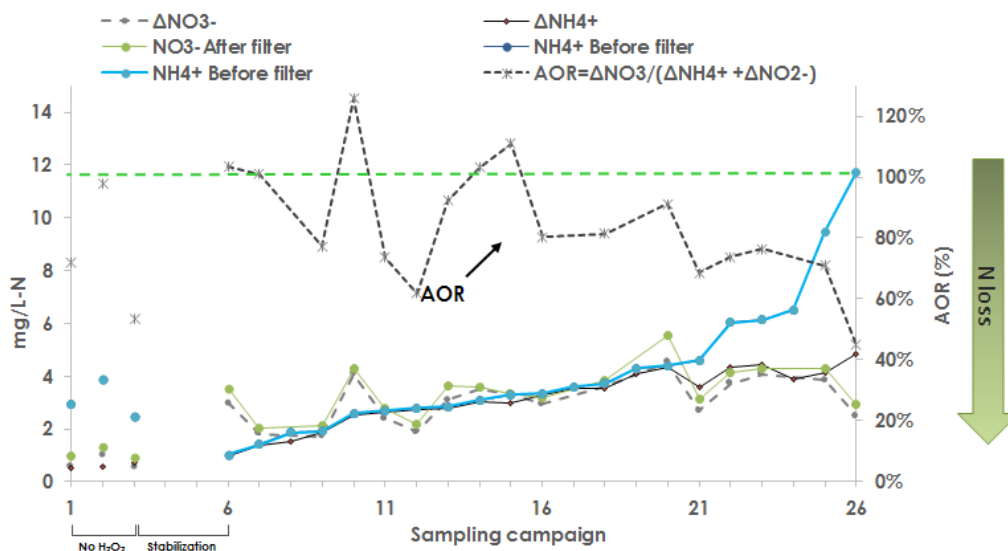


Figure 2. Concentrations of NH_4^+ before and after the filter, NO_3^- after the filter, and the delta of NH_4^+ and NO_3^- (mg/L-N) are presented. The gray dashed line represents the NH_4^+ oxidation rate, which is the ratio between the introduced NO_3^- and the sum of the removed NH_4^+ and NO_2^- (%). The green dashed line represents the complete (100%) calculated mass balance between removed NH_4^+ and NO_2^- and introduced NO_3^- . The sampling campaigns were sorted by feed values of NH_4^+ . The first three values represent the control without H_2O_2 addition.

Moreover, the calculated AOR was less than $\sim 70\%$ when NH_4^+ values at the BF sampling point were higher than 4 mg/L-N. Values over 100% can be explained by the contribution of NH_4^+ via a higher

rate of organic nitrogen (amino acids) decomposition than nitrification. The relatively low removal rates of organic compounds by the biofilter when H_2O_2 was added, in comparison to NH_4^+ and NO_2^- , suggests that the level of organic carbon degradability was a limiting factor in favoring oxygen utilization for nitrification on the one hand and carbon utilization for denitrification on the other.

3.6. Mass Balance

Calculations of the total nitrogen mass balance are presented in Figure 3, considering organic nitrogen values, revealed an average nitrogen loss of 2.24 ± 1 mg-N/L with H_2O_2 and 0.25 ± 0.06 mg-N/L at the control. In addition, a higher nitrogen loss was calculated in parallel to the increase in NH_4^+ concentration at the inlet. Calculations to evaluate the nitrogen loss in favor of assimilation with H_2O_2 addition revealed that the assimilation rate was around 50% from all nitrogen removed (Table A1). This indicates that significant nitrogen loss was due to anoxic activity in the biofilter, which occurred simultaneously with nitrification. In addition, denitrification credit, the calculated oxygen that was credited due to utilization of NO_3^- as electron acceptor, was significant and varied between 1–7 mg/L of COD and also increased in parallel to the increase in NH_4^+ concentrations at the inlet. To explain the higher nitrogen loss under aerobic conditions that was enhanced by the oxygen surplus as H_2O_2 , we hypothesized that H_2O_2 , due to a lack of solubility limitations, better penetrates into the depth of the biofilm, decomposes, and stimulates activity.

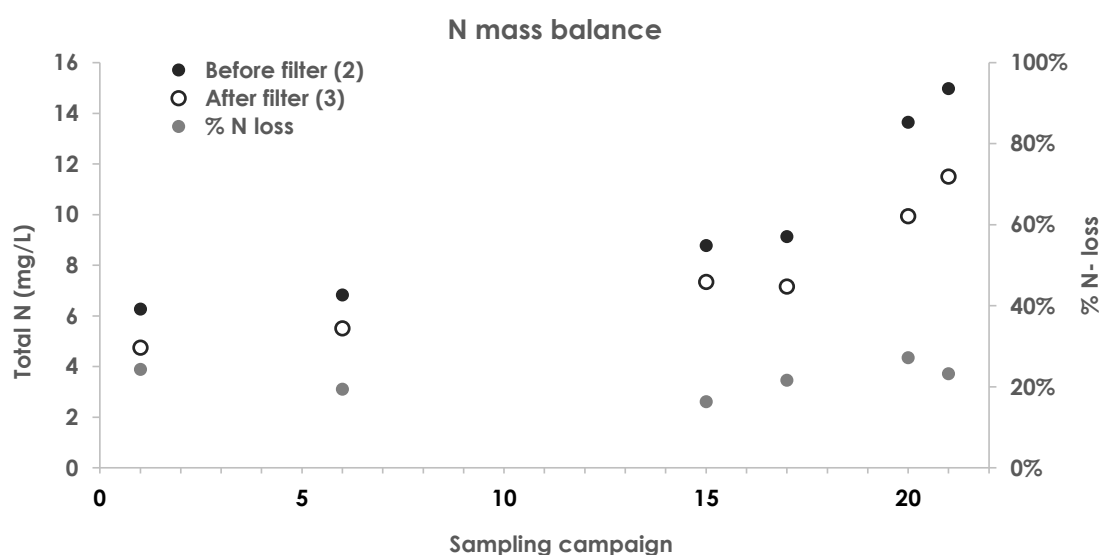


Figure 3. Accumulated inorganic and organic nitrogen concentrations (mg/L-N) before (BF) and after (AF) the biofilter and removal rates (%).

3.7. Functional Potential of the Biomass

The Metagenomics performed on the sample yielded 8.2 M high-quality reads, out of which, 3.6 M were aligned to ~1250 organisms, when >98% are bacteria, both in the abundance and number of strains. The resulting outcome indicated a highly diverse bacterial community, with a calculated Shannon diversity index value of 5.6 as opposed to the theoretical value of 7.13 for a sample with equal diversity. The relative abundance of functional genes in the biofilter biomass is presented in Figure 4. The relative abundance of genes involved in nitrification (AmoA and NxrB) was higher, by 3 to 4 orders of magnitude, than the genes involved in other electron donor pathways (as drsEFH or aprA). In addition, the log relative abundance of the genes involved in denitrification and oxygen utilization (cyt c oxidases) was also significantly higher in comparison to the other various metabolic pathways examined.

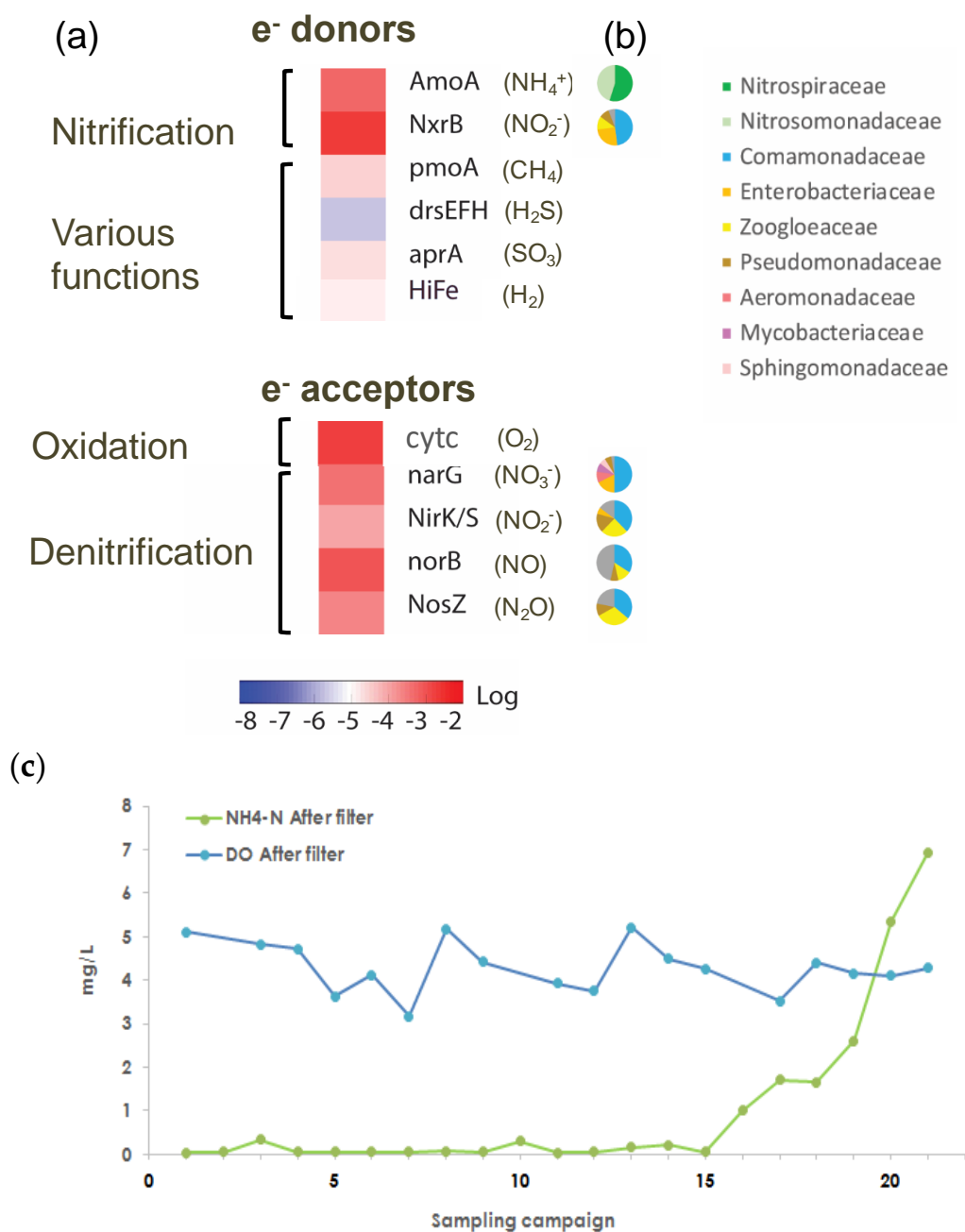


Figure 4. Log-transformed relative abundances of the marker genes of enzymes involved in nitrification, denitrification, and other metabolic pathways in the biofilter while H₂O₂ was added with various electron donors and acceptors (a). For each functional gene, the composition of classified genera is presented (b). Concentrations of ammonia and oxygen in the system outlet (c).

Considering that *cyt c* is harbored by AOB (nitrification) [45], as well as denitrifying organisms (denitrification) [46], the relative high abundance of this gene is consistent with the experimental results of simultaneous nitrification and denitrification activity (Figure 2). The higher relative abundance obtained for the gene of NO₂⁻ oxidation (*nxrB*) over NH₄⁺ oxidation, might suggest the possible occurrence of a “ping pong” mechanism of cyclic NO₂⁻ oxidation and reduction, resulting in a higher NO₂⁻ oxidation rate than NH₄⁺ [47]. In parallel, the composition of identified genera of each of the N related genes (Figure 4b) revealed a variety of heterotrophs capable of conducting denitrification, when the genera belonging to the family *Comamonadaceae* was the most dominant one. Interestingly, the identified genus related to NH₄⁺ oxidation was related to AOB and NOB, while the identified

genus related to NO_2^- oxidation was of heterotrophs. This might suggest that the involvement of commamox and heterotrophs in nitrification [48–50].

The comparison of the functional potential of the microbial community reflects clear dominance for N biotransformation by simultaneous nitrification and denitrification. The significant anoxic potential reflected from the relative abundance of functional genes can be explained by the denitrifying community capable of being active at the presence of oxygen (low half-saturation rate of oxygen inhibition, $K_{\text{OI}} = 0.1\text{--}0.2$ mg/L) [43].

Moreover, favoring oxygen utilization for nitrification, with a C/N ratio similar to wastewater, can be explained by the selection of organisms that are more competitive and characterized with a low substrate half-saturation rate coefficient ($K_{\text{ONitrosospira}} = 0.1\text{--}0.2$ mg/L, $K_{\text{OAOB}} = 0.26\text{--}0.15$ mg/L), which is more typical to nitrifiers in comparison to heterotrophs [51,52]. Jiang et al. (2013) also observed that the increase in oxygen availability in the upflow biofilter resulted in utilization by nitrifiers rather than heterotrophic biomass [19].

We suggest that the typical low biodegradability of the organic carbon at the secondary effluent, which was also reflected in the low removal rate of the COD, BOD, and UVA_{254} , mentioned earlier (Section 3.4, Figure A5a,b in the Appendix A) was a key parameter on the rates of heterotrophic activity [44].

The environmental conditions of a low degradability rate of the organic matter and the addition of oxygen via H_2O_2 , could be a possible explanation for favoring NH_4^+ rather than organic material oxidation. Such conditions, may promote simultaneous nitrification/nitrogen-removal activity. The significant relative abundance of genes with the potential for NO_2^- oxidation on one hand and NO_2^- reduction on the other hand strongly suggest that competition for NO_2^- is a key in the dynamics of the community structure and function.

To address the paradox of excess oxygen availability in the reactor, due to H_2O_2 addition and degradation, while the relative abundance of genes related to anoxic activity reflects conditions of limited oxygen, we hypothesize that this community structure reflects inner localization in the biofilm: Whereas AOB and NOB are localized at the outer layer of the biofilm, degrade the H_2O_2 , and utilize the supplemental oxygen for nitrification, in parallel with the depletion of oxygen along the depth of the biofilm, NO_2^- and NO_3^- are reduced. It is also possible that the nitrifiers are located in the pockets inside the biofilm and the better mass transfer of H_2O_2 enables utilization in a deeper location. We also suggest that the bacterial community that was investigated in this study indicates maximized thermodynamic utilization of electron acceptors and donors, with significant rates of anoxic activity.

The limitation of the process performance under increasing loads of NH_4^+ might be due to a lack of oxygen, limited HRT, or reactor volume and should be further investigated. As mentioned in previous research [34] the biofilter system succeeded in decreasing the oxygen demand and the drop in the ORP in following SAT. We suggest that the design presented in this study could be beneficial for treating secondary effluents containing residual levels of NH_4^+ (few mg/L-N), which is required to be removed under discharge or reuse restrictions.

4. Discussion

We suggest a model to describe the biokinetics of tertiary wastewater biofiltration systems with the addition of H_2O_2 . The model focuses on the soluble (not particulate) content, carbon content similar to the secondary effluent (low biodegradability, nitrogen content), and the significance of metabolism over assimilation (Appendix A.1 and Table A1). Generally, although some full reduction of NO_3^- to NH_4^+ may occur simultaneously, it is neglected in the model.

The model suggest that the addition of H_2O_2 (Figure 5) promoted the rates of the following pathways: (i) nitrification and (ii) nitratation, which occurs at high rates, and (iii) biodegradable COD oxidation, which occurs at minor rates. In parallel, (v) NO_2^- and (vi) NO_3^- reduction via denitrification and (vii) are also stimulated.

Appendix A

Appendix A.1 Theoretical Calculation of and Oxygen Nitrogen Mass Balance

Nitrogen mass balance was calculated by making the following assumptions: (1) ammonia was the only nitrogen source for assimilation for biomass growth, (2) full aerobic utilization of oxygen originated from H_2O_2 , (3) full nitrification to nitrate as the only electron acceptor for denitrification and (4) all nitrogen loss originated in anoxic denitrification activity. Two values for yields of 0.6 mg COD biomass/mg substrate COD (aerobic) as the upper limit and 0.4 mg COD biomass/mg substrate COD (anoxic) [43] as the lowest limit were used in the calculations as heterotroph activity was probably both aerobic and anoxic.

$$N_{\text{loss}} = BF_{\text{Inlet}} [\text{mg/L TKN-N} + \text{mg/L NO}_2^- \text{N} + \text{mg/L NO}_3^- \text{N}] - AF_{\text{Outlet}} [\text{mg/L TKN-N} + \text{mg/L NO}_2^- \text{N} + \text{mg/L NO}_3^- \text{N}] \quad (\text{A1})$$

$$\text{OHO Nitrogen assimilated mg/L} = \Delta \text{COD} \times Y_{\text{OHO}} \times 14 (\text{N gr/mole}) / 113 (\text{Biomass gr/mole}) \quad (\text{A2})$$

$$N_{\text{loss denitrification}} = \sum \Delta N_{\text{loss}} - \text{Nitrogen assimilated mg/L} \quad (\text{A3})$$

$$\text{Denitrification credit} = N_{\text{loss denitrification}} \times 2.8 \text{ mg COD/mg NO}_3^- \text{N} [43] = \Delta \text{COD}_{\text{denitrification}} \quad (\text{A4})$$

The data presents the delta between the inlet and outlet: ΔNH_4^+ , ΔNO_2^- , ΔNO_3^- , ΔCOD , $\Delta \Sigma \text{N}$ including Organic nitrogen (TKN).

Oxygen mass balance was calculated by making the following assumptions:

- (1) All oxygen transformations were biological.
- (2) All the degradation of H_2O_2 was biologically with oxygen and water as the only by products (based on previous lab calibrations).
- (3) Excess oxygen, over the dissolved oxygen, in the inlet water was originated from H_2O_2 degradation.

$$\text{Degradation of } 27 \text{ mg/L } H_2O_2 = 12.7 \text{ mg } O_2 (1/0.47) \quad (\text{A5})$$

$$O_2 \text{ demand for full nitrification} = 4.57 \text{ mg } O_2/\text{mg-N} \quad (\text{A6})$$

$$O_2 \text{ mass balance } \Delta O_2 = (\text{DO}_{\text{inlet}} + 27 \text{ mg/L } H_2O_2 \times 0.47) - \text{DO}_{\text{outlet}} \quad (\text{A7})$$

$$\text{Potential oxygen consumed for nitrification} = \Delta O_2 - O_2 \text{ demand for nitrification } (\Delta \text{NH}_4 \times 4.57) \quad (\text{A8})$$

The theoretical demand of $H_2O_2/\text{mg-N } NH_4$ for full nitrification was calculated as follows:

$$C_{H_2O_2} \times 0.47 (\text{mg } O_2/\text{mg } H_2O_2) \times 4.57 (\text{mg } O_2/\text{mg-N}) = 9.72 \text{ mg of } H_2O_2/\text{mg-N } NH_4 \quad (\text{A9})$$

A significant difference was obtained between the calculated concentrations of nitrogen assimilated with or without H_2O_2 , in both estimates (0.8–1.15 mg/L-N vs 0.17–0.25 mg/L-N). Non-assimilative N loss (denitrification) was also significant with H_2O_2 (3–4 mg/L-N) while the calculated values of the control were within an error of measurement. This indicated significant enhancement of microbial growth and anoxic activity by H_2O_2 addition.

Considering the difference between the ammonia removed (theoretically oxidized to the oxygen balance it can be clearly seen that more NH_4^+ was consumed than oxygen was available along the increase in NH_4^+ concentration (negative values of mass balance).

Table A1. Nitrogen mass balance of the biofilter system with and without H₂O₂.

	# Campaign	N Loss (mg-N/L)	OHO Assimilation (mg-N/L)	N Loss for Denitrification (mg-N/L)	Denitrification Credit (COD mg/L Utilized for Denitrification)
OHO Yield = 0.6	0	1.52	1.04	0.48	1.3
	6	1.32	0.82	0.50	1.4
	15	1.43	1.04	0.39	1.1
	17	1.97	1.26	0.71	2.0
	20	3.71	1.64	2.07	5.8
	21	3.47	1.12	2.36	6.6
	Average H ₂ O ₂	2.24	1.15	1.09	3.0
	STD dev. H ₂ O ₂	0.98	0.25	0.81	2.27
	28	0.32	0.30	0.02	0.1
	29	0.25	0.15	0.10	0.3
	30	0.18	0.30	0.00	0.0
	Average Control	0.25	0.25	0.04	0.1
	STD dev Control	0.06	0.07	0.04	0.12
	# Campaign	N Loss (mg-N/L)	OHO Assimilation (mg-N/L)	N Loss for Deni (mg-N/L)	Denitrification Credit (COD mg/L Utilized for Deni)
OHO Yield = 0.4	0	1.52	0.69	0.83	2.3
	6	1.32	0.74	0.58	1.6
	15	1.43	0.69	0.74	2.1
	17	1.97	0.84	1.13	3.2
	20	3.71	1.09	2.62	7.3
	21	3.47	0.74	2.73	7.6
	Average H ₂ O ₂	2.24	0.80	1.44	4.0
	STD H ₂ O ₂	0.98	0.14	0.89	2.50
	28	0.32	0.20	0.12	0.3
	29	0.25	0.10	0.15	0.4
	30	0.18	0.20	0.00	0.0
	Average Control	0.25	0.17	0.09	0.3
	STD dev. Control	0.06	0.05	0.07	0.18

Notes: denitrification refers to denitrification.

Table A2. Oxygen mass Balance of the biofilter system with and without H₂O₂.

# Campaign	O ₂ Inlet (mg-/L)	O ₂ Outlet (mg-/L)	O ₂ from H ₂ O ₂	O ₂ Balance (Consumed)	Delta NH ₄	Potential Oxygen Consumed for Nitrification
1	3.79	5.1	12.7	11.39	0.98	6.92
2			12.7	12.70	1.35	6.53
3	5.53	4.83	12.7	13.40	1.54	6.37
4	5	4.72	12.7	12.98	1.85	4.53
5	3.87	3.62	12.7	12.95	2.55	1.30
6	3.8	4.12	12.7	12.40	2.63	0.37
7	3.43	3.18	12.7	12.95	2.75	0.38
8	6.30	5.17	12.7	13.83	2.77	1.16
9	5.38	4.42	12.7	13.66	3.05	-0.28
10			12.7	12.70	3.00	-1.01
11	4.69	3.92	12.7	13.47	3.30	-1.61
12	3.92	3.75	12.7	12.87	3.55	-3.35
13	5.83	5.2	12.7	13.32	3.56	-2.93
14	4.1	4.49	12.7	12.26	4.08	-6.39
15	6.15	4.27	12.7	14.58	4.35	-5.30
16	5.13	3.53	12.7	14.30	3.60	-2.15
17	4.50	4.41	12.7	12.79	4.32	-6.94
18	3.83	4.16	12.7	12.37	4.46	-8.00
19	5.67	4.10	12.7	14.27	3.90	-3.55
20	5.48	4.28	12.7	13.90	4.12	-4.94

Appendix A.2 The Backwash Cycle

Periodic backwashing included combining air/water followed by water backwashing (Figure 1). The backwash cycle consisted of a short backwash to release filter-bed clogging by the air–water backwash, and another 10 min of water backwash and downflow wash to the sewer before restarting the filter. Backwashing volume was ~1.3% of the total volume filtered. The bottom plate nozzles were removed to improve the mixing efficiency and a side stream was also recirculated to the bottom part thus forming a sludge blanket which improved flocculation (verified by PSD analysis). The head loss was limited by online control to 0.5 bar/cycle and in the case of higher head loss, a second automatic backwash was performed. The quality of filtration was observed by the stable performance with low outlet turbidity (0.4–0.8 NTU).

Appendix A.3 Water Parameters Methodology

The water quality of the samples was conducted in the SHAFDAN lab using selective electrode 4500-NH₃ for ammonium, 4500-NO₂-B colorimetric method for nitrite, 4110B ion chromatography for nitrate with chemical suppression of eluent conductivity, 5910B ultraviolet absorption method for UV absorbance at 254 nm (UVA), 5310B high-temperature combustion method for dissolved organic carbon (DOC), 4500-O C azide modification for DO, 5220B open reflux method for chemical oxygen demand (COD) and NOVA 60 kit for H₂O₂.

Appendix A.4 H₂O₂ Decomposition

Generally, the reaction occurs in two distinct stages in the catalytic reaction pathway. First, oxidation of the enzyme by one molecule of H₂O₂, while the oxygen–oxygen bond in peroxide is cleaved. At the second stage, another molecule of H₂O₂ reacts with the bond oxygen ion and forms molecular oxygen and water [28].

Appendix A.5 Secondary Effluent Particle Analysis

Effluent particles and aggregates were analyzed by Micro Flow Imaging. In brief, a fluid sample is drawn through a flow cell, illuminated with a light-emitting diode at 470 nm, and the magnified image is captured by digital camera. This image is then automatically analyzed to determine the particles' equivalent circular diameter (ECD) which represents the diameter of a sphere that occupies the same two-dimensional surface area as the particle. Analysis was conducted on particles of between ~2 and 400 μm.

Appendix A.6 Particles Distribution

A typical PSD analysis of the secondary effluent after 500 μm, post flocculation and after the biofilter is presented in Figure A1.

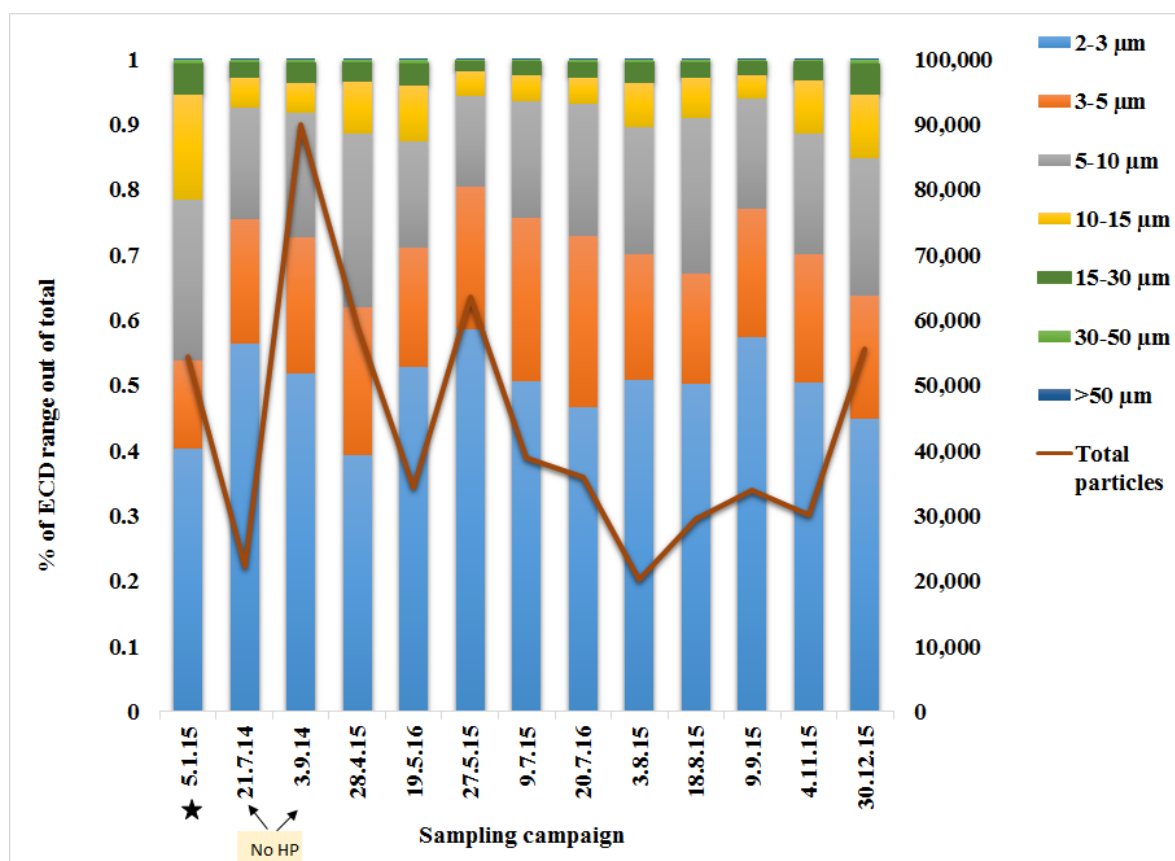


Figure A1. Particle distribution analysis over sampling campaigns. The Particle size is represented as an equivalent circular diameter (ECD). Total particle concentration (#/mL) is plotted as a red line. The results presented at Figure 2 refer to the campaign marked with a star. No HP is related to control runs without the addition of H₂O₂.

Appendix A.7 Media Sampling and Metagenome Analysis

The metagenome analysis was conducted to investigate the functional potential of the microbial media community. At the middle of the operation cycle (6 h) the biofilter was emptied and a sample of 50 g anthracite media was taken from a depth of 40 cm from the top of the media, thoroughly mixed for homogenization and immediately stored in dry ice. DNA from the media was extracted using Exgene Soil DNA Mini Kit. Whole-genome (shotgun) libraries were prepared using the TruSeq DNA PCR-Free HT Library Preparation Kit (Illumina, San Diego, CA, USA) and sequenced using an Illumina MiSeq benchtop sequencer with a target fragment length of 250 bp.

The final outputs of the metagenomics sequencing were modified using Cutadapt [55] to remove adapters and low-quality reads, and contigs were created using IDBA-UD [56]. A total of 8.9 M reads, was produced. The construction of a non-redundant gene catalog and the quantification of reference gene abundance (Gene calling) on the assembled scaffolds was performed using Prodigal [57]. Predicted genes were clustered using UCLUST [58]. High-quality reads were mapped to the reference gene catalog using BWA [59]. Mapped reads were used to form an abundance vector of the number of reads mapped to each gene. This was normalized based on data set size and gene length. Annotation was done using USEARCH [58] against the NCBI database (best hit with $E=1e-5$, Bitscore >60 and sequence similarity $>30\%$). Genus annotation was done using BWA aligner against the entire NCBI genome database ($\sim 80,000$ genomes) and using PathoScope 2.0 [60] to quantify proportions of contigs from individual strains.

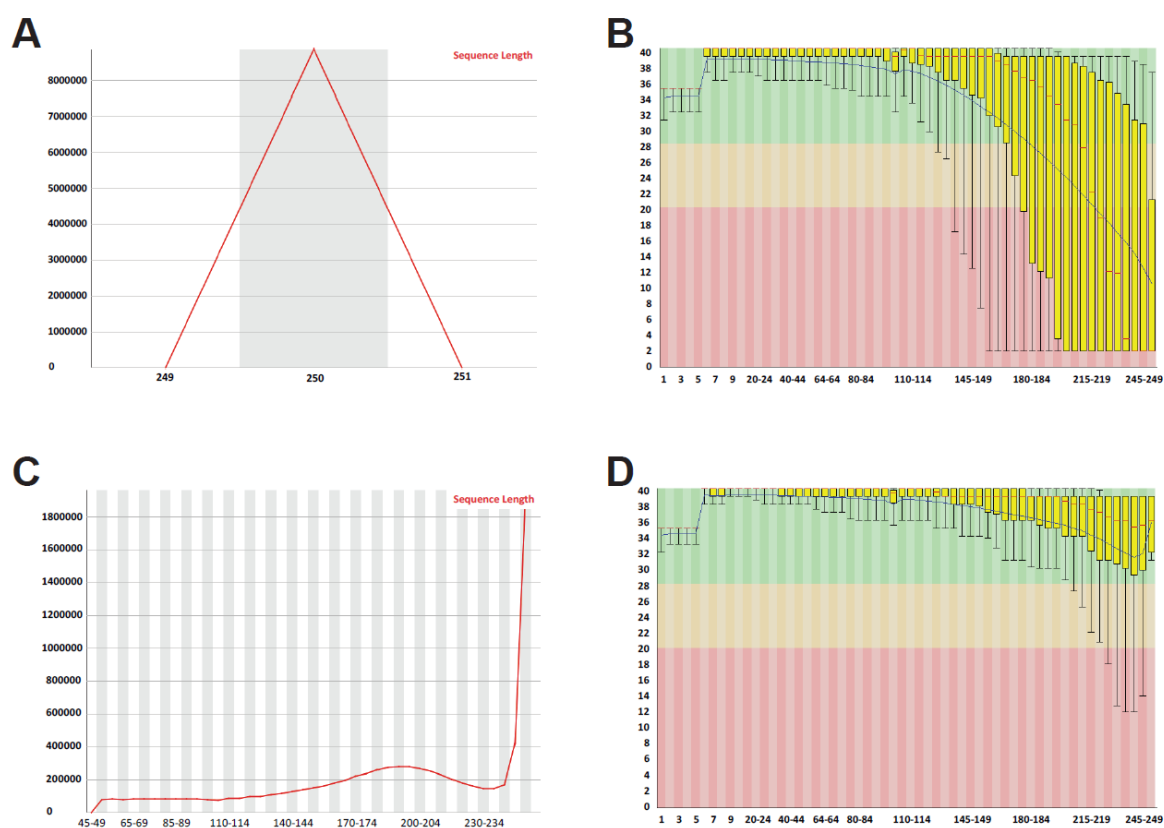


Figure A2. Metagenomics quality and length distribution: (A,B) before applying Cutadapt (Martin 2017): length distribution (A) and box plot distribution of quality score (Phred) (B). (C,D)—length and Phred distribution after applying Cutadapt.

Appendix A.8 Functional Molecular Analysis of the Biomass

The diversity of species within the sample indicating low diversity of the community in the sample. The number of reads that were aligned to nitrogen-related species were 43% of the total aligned reads,

reflecting significant functional potential for the nitrogen cycle in the sampled bacterial community. Gene catalog was extracted from NCBI's nucleotide database. Mapped reads were subsequently filtered by removing those with a poor alignment ($-q30$). The remaining mapped reads were used to form an abundance matrix of the number of reads mapped to each gene in every sample. The abundance matrix was normalized based on data set.

Genes aligning to the reads were sorted according to their respective identified organisms which varied between 6%–19% among all the reads related to each gene (Figure A3).

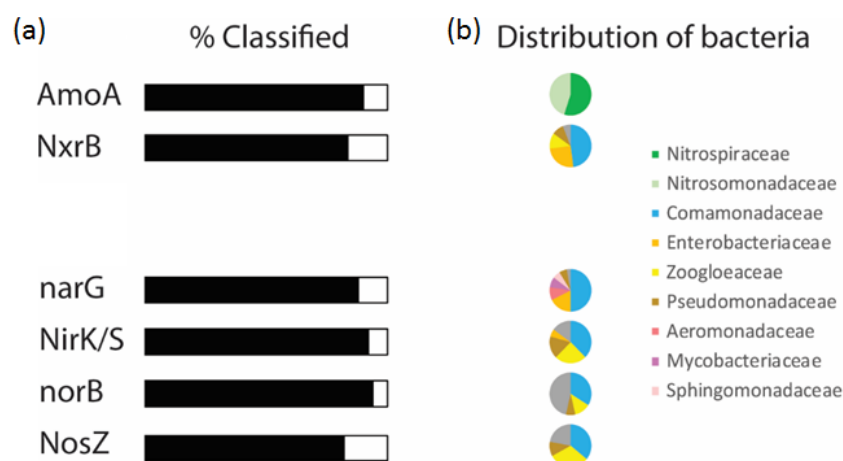


Figure A3. Percentage of classified (white) and unclassified (black) reads out of all the reads of each gene (a) and the composition of the identified genus of each gene (b).

Appendix A.9 Biofilter Performance—Particle Analysis

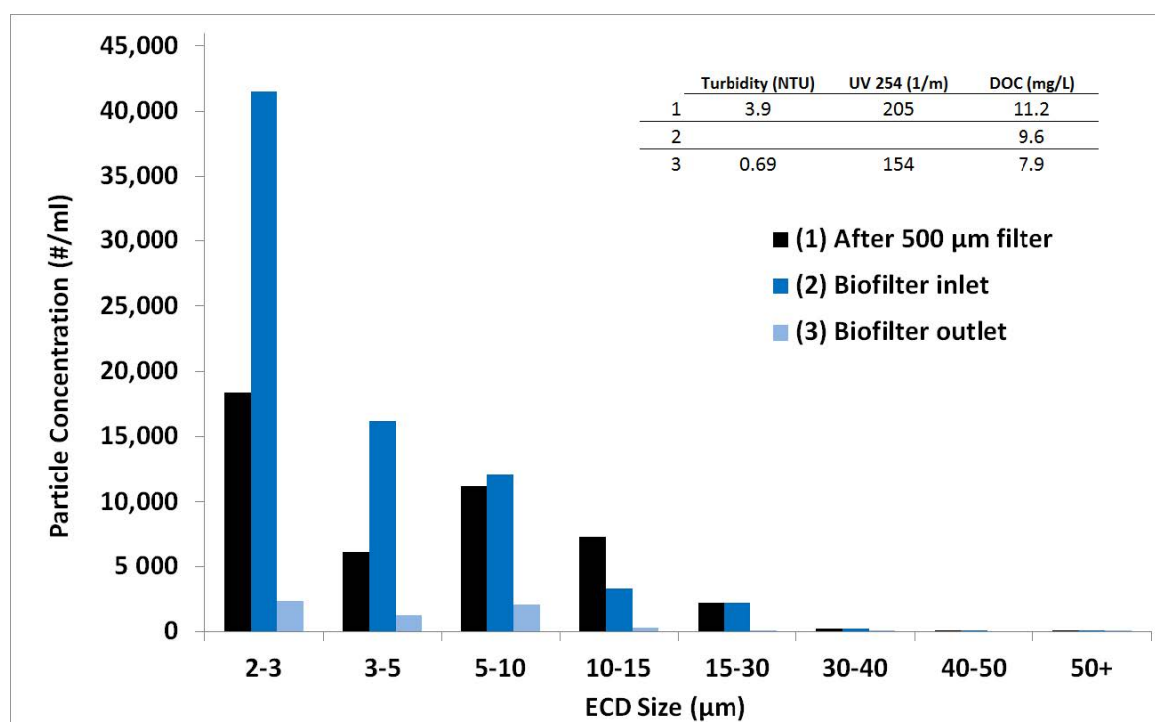


Figure A4. Particle-size distribution (PSD) analysis of a representative sampling campaign with H₂O₂. A comparison between sampling points after 500µm filtration (1) at the inlet of the biofilter after coagulation and flocculation (2) and at the outlet of the biofilter (3).

Flocculation before biofiltration increased particle counts, due to flocculation of the macromolecules and colloid particles ($<2 \mu\text{m}$) which were not analyzed. As expected, particle concentration decreased dramatically after biofiltration for all ECDs.

Appendix A.10 Organic Carbon Performance

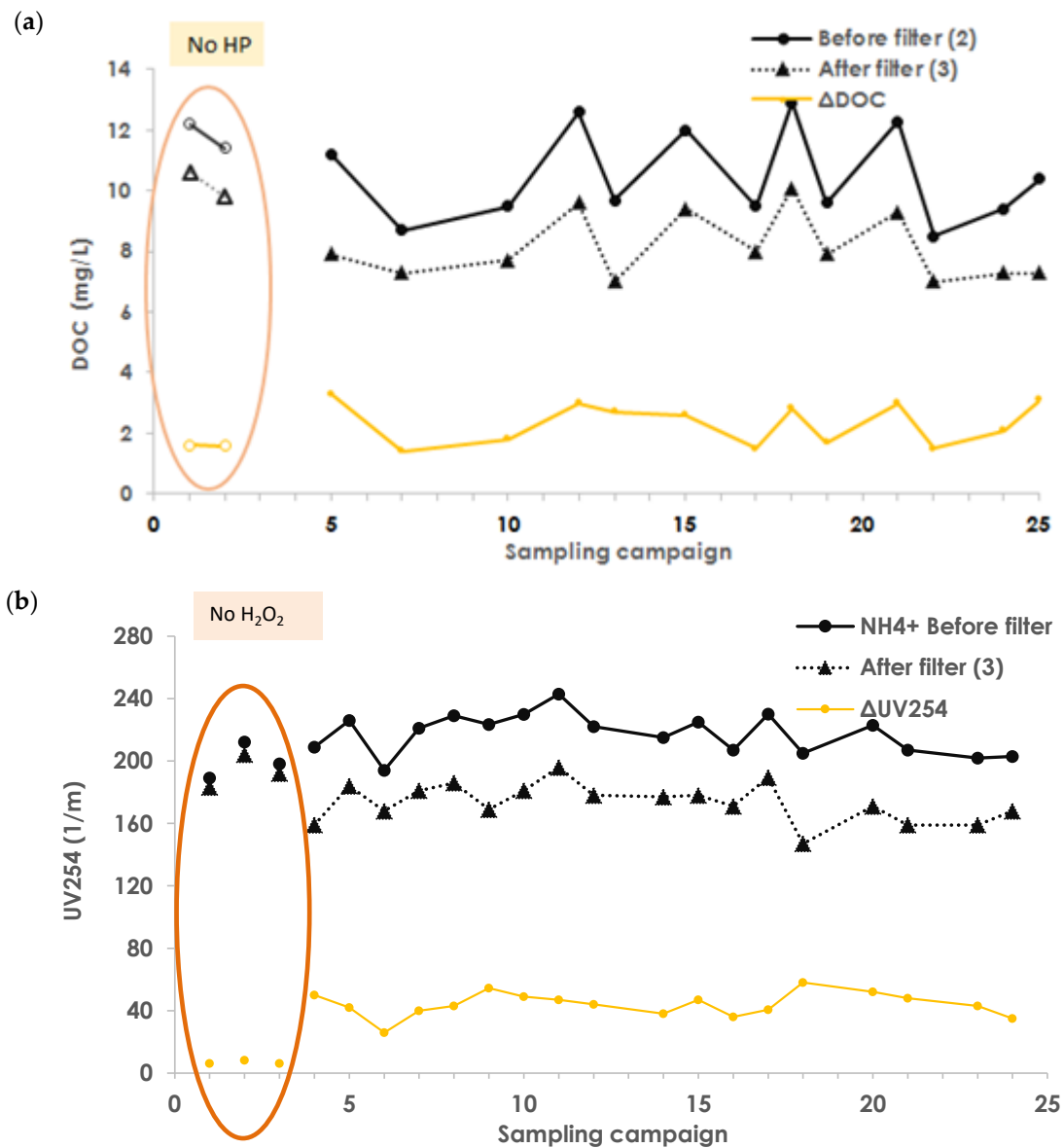


Figure A5. Concentrations and the removal of DOC (a) and UVA (UV₂₅₄) (b) over sampling campaigns before the biofilter (BF) and after the biofilter (AF), which was also sorted by feed values of ammonium during experiments with H₂O₂ addition. Reference campaigns of no H₂O₂ are circled in orange.

Appendix A.11 Nitrite Removal and Concentration

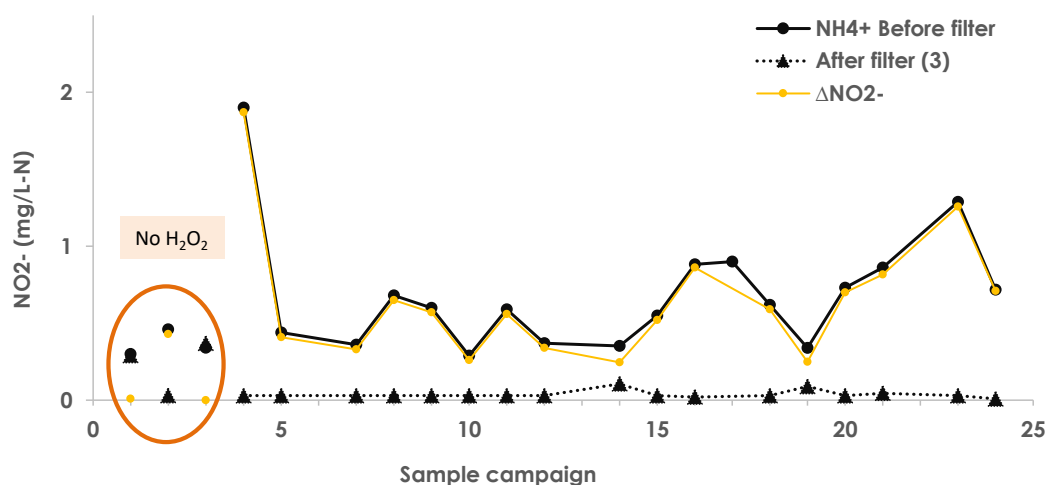


Figure A6. Concentrations and removal of nitrite (mg/L-N) over sampling campaigns, before the biofilter (BF) and after the biofilter (AF) with H_2O_2 addition, also sorted by feed values of ammonium. No H_2O_2 campaigns are circled in orange.

References

- Bixio, D.; De Hayder, B.; Cikurel, H.; Muston, M.; Miska, V.; Joksimovic, D.; Schäfer, A.I.; Ravazzini, A.; Aharoni, A.; Savic, D.; et al. Municipal wastewater reclamation: Where do we stand? An overview of treatment technology and management practice. *Water Sci. Technol. Water Supply* **2005**, *5*, 77–86. [CrossRef]
- Siegel, S.M. *Let There Be Water: Israel's Solution for a Water-Starved World*; Thomas Dunne Books/St. Martin's Press: New York, NY, USA, 2015; ISBN 978-1-250-07395-2.
- Emerging Technologies for Wastewater Treatment and In-Plant Wet Weather Management*; U.S Environmental Protection Agency (EPA): Washington DC, USA, 2013; Volume 832.
- Tchobanoglous, F.B.G. *Wastewater Engineering and Reuse*, 4th ed.; McGraw-Hill: New York, NY, USA, 2003; ISBN 978-1-259-01079-8.
- Van Den Akker, B.; Holmes, M.; Cromar, N.; Fallowfield, H. Application of high rate nitrifying trickling filters for potable water treatment. *Water Res.* **2008**, *42*, 4514–4524. [CrossRef]
- Miska-Markusch, V. *Effluent Filtration for more than Particle Removal*; Leibniz Universität Hannover: Hannover, Germany, 2009.
- Müller, J.; Drewes, J.E.; Hübner, U. Sequential biofiltration—A novel approach for enhanced biological removal of trace organic chemicals from wastewater treatment plant effluent. *Water Res.* **2017**, *127*, 127–138. [CrossRef]
- Alidina, M.; Li, D.; Drewes, J.E. Investigating the role for adaptation of the microbial community to transform trace organic chemicals during managed aquifer recharge. *Water Res.* **2014**, *56*, 172–180. [CrossRef]
- Palomo, A.; Fowler, S.J.; Gülay, A.; Rasmussen, S.; Sicheritz-Ponten, T.; Smets, B.F. Metagenomic analysis of rapid gravity sand filter microbial communities suggests novel physiology of *Nitrospira* spp. *ISME J.* **2016**, *10*, 2569–2581. [CrossRef]
- Pinto, A.J.; Marcus, D.N.; Ijaz, Z.; Bautista-de los Santos, Q.M.; Dick, G.J.; Raskin, L. Metagenomic Evidence for the Presence of Comammox *Nitrospira*-Like Bacteria in a Drinking Water System. *mSphere* **2015**, *1*, e00054-15. [CrossRef]
- Salerno, C.; Berardi, G.; Laera, G.; Pollice, A. Functional Response of MBR Microbial Consortia to Substrate Stress as Revealed by Metaproteomics. *Microb. Ecol.* **2019**, *78*, 873–884. [CrossRef]
- Salerno, C.; Benndorf, D.; Kluge, S.; Palese, L.L. Metaproteomics Applied to Activated Sludge for Industrial Wastewater Treatment Revealed a Dominant Methylotrophic Metabolism of *Hyphomicrobium zavarzinii*. *Microb. Ecol.* **2016**, *72*, 9–13. [CrossRef]

13. Mendoza-Espinoza, L.; Stephenson, T. A Review of Biological Aerated Filters (BAFs) for Wastewater Treatment. *Environ. Eng. Sci.* **1999**, *16*, 201–216. [[CrossRef](#)]
14. Rassamee, V.; Sattayatewa, C.; Pagilla, K.; Chandran, K. Effect of oxic and anoxic conditions on nitrous oxide emissions from nitrification and denitrification processes. *Biotechnol. Bioeng.* **2011**, *108*, 2036–2045. [[CrossRef](#)]
15. Yoo, H.; Ahn, K.; Lee, H.J.; Lee, K.; Kwak, Y.; Song, K. Nitrogen removal from synthetic wastewater by simultaneous nitrification and denitrification (SND) via nitrite in an intermittently-aerated reactor. *Water Res.* **1999**, *33*, 145–154. [[CrossRef](#)]
16. Bassin, J.P.; Abbas, B.; Vilela, C.L.S.; Kleerebezem, R.; Muyzer, G.; Rosado, A.S.; van Loosdrecht, M.C.M.; Dezotti, M. Tracking the dynamics of heterotrophs and nitrifiers in moving-bed biofilm reactors operated at different COD/N ratios. *Bioresour. Technol.* **2015**, *192*, 131–141. [[CrossRef](#)]
17. de Vet, W.W.J.M.; Kleerebezem, R.; van der Wielen, P.W.J.J.; Rietveld, L.C.; van Loosdrecht, M.C.M. Assessment of nitrification in groundwater filters for drinking water production by qPCR and activity measurement. *Water Res.* **2011**, *45*, 4008–4018. [[CrossRef](#)]
18. Yu, X.; Qi, Z.; Zhang, X.; Yu, P.; Liu, B.; Zhang, L.; Fu, L. Nitrogen loss and oxygen paradox in full-scale biofiltration for drinking water treatment. *Water Res.* **2007**, *41*, 1455–1464. [[CrossRef](#)]
19. Jiang, B.; Hu, W.; Pei, H.; Chen, P.; Liu, Q. The influence of aeration on nitrification and the nitrifier distribution in an upflow biological aerated filter for tertiary treatment of municipal sewage. *Desalin. Water Treat.* **2010**, *24*, 308–320. [[CrossRef](#)]
20. Albuquerque, A.; Makinia, J.; Pagilla, K. Impact of aeration conditions on the removal of low concentrations of nitrogen in a tertiary partially aerated biological filter. *Ecol. Eng.* **2012**, *44*, 44–52. [[CrossRef](#)]
21. Matsumoto, S.; Terada, A.; Tsuneda, S. Modeling of membrane-aerated biofilm: Effects of C/N ratio, biofilm thickness and surface loading of oxygen on feasibility of simultaneous nitrification and denitrification. *Biochem. Eng. J.* **2007**, *37*, 98–107. [[CrossRef](#)]
22. Brindle, K.; Stephenson, T.; Semmens, M.J. Nitrification and oxygen utilisation in a membrane aeration bioreactor. *J. Memb. Sci.* **1998**, *144*, 197–209. [[CrossRef](#)]
23. Pellicer-Nàcher, C.; Smets, B.F. Structure, composition, and strength of nitrifying membrane-aerated biofilms. *Water Res.* **2014**, *57*, 151–161. [[CrossRef](#)]
24. Fiorenza, S.; Ward, C.H. Microbial adaptation to hydrogen peroxide and biodegradation of aromatic hydrocarbons. *J. Ind. Microbiol. Biotechnol.* **1997**, *18*, 140–151. [[CrossRef](#)]
25. Zappi, M.; White, K.; Hwang, H.-M.; Bajpai, R.; Qasim, M. The Fate of Hydrogen Peroxide as an Oxygen Source for Bioremediation Activities within Saturated Aquifer Systems. *J. Air Waste Manag. Assoc.* **2000**, *50*, 1818–1830. [[CrossRef](#)]
26. Chance, B.; Herbert, D. The enzyme-substrate compounds of bacterial catalase and peroxides. *Biochem. J.* **1950**, *46*, 402–414. [[CrossRef](#)]
27. Northrop, J.H. Experimental Conditions and General Results. Effect of Varying the Concentration of Catalase. *J. Gen. Physiology* **1924**, *5*, 373–387.
28. Sooch, B.S.; Kauldhar, B.S.; Puri, M. Recent insights into microbial catalases: Isolation, production and purification. *Biotechnol. Adv.* **2014**, *32*, 1429–1447. [[CrossRef](#)]
29. Flores, M.J.; Brandi, R.J.; Cassano, A.E.; Labas, M.D. Chemical disinfection with H₂O₂—The proposal of a reaction kinetic model. *Chem. Eng. J.* **2012**, *198–199*, 388–396. [[CrossRef](#)]
30. Lakretz, A.; Ron, E.Z.; Mamane, H. Biofilm control in water by a UV-based advanced oxidation process. *Biofouling* **2011**, *27*, 295–307. [[CrossRef](#)]
31. Tusseau-Vuillemin, M.H.; Lagarde, F.; Chauviere, C.; Hedit, A. Hydrogen peroxide (H₂O₂) as a source of dissolved oxygen in COD-degradation respirometric experiments. *Water Res.* **2002**, *36*, 793–798. [[CrossRef](#)]
32. Lakretz, A.; Ron, E.Z.; Harif, T.; Mamane, H. Biofilm control in water by advanced oxidation process (AOP) pre-treatment: Effect of natural organic matter (NOM). *Water Sci. Technol.* **2011**, *64*, 1876–1884. [[CrossRef](#)]
33. Yang, Y.; Cheng, D.; Li, Y.; Yu, L.; Gin, K.Y.H.; Chen, J.P.; Reinhard, M. Effects of monochloramine and hydrogen peroxide on the bacterial community shifts in biologically treated wastewater. *Chemosphere* **2017**, *189*, 399–406. [[CrossRef](#)]
34. Zucker, I.; Mamane, H.; Cikurel, H.; Jekel, M.; Hubner, U.; Avisar, D. A hybrid process of biofiltration of secondary effluent followed by ozonation and short soil aquifer treatment for water reuse. *Water Res.* **2015**, *84*, 315–322. [[CrossRef](#)]

35. Cikurel, H.; Rebhun, M.; Amirtharajah, A.; Adin, A. Wastewater effluent reuse by in-line flocculation filtration process. *Water Sci. Technol.* **1996**, *33*, 203–211. [[CrossRef](#)]
36. Mamane, H.; Kohn, C.; Adin, A. Characterizing Shape of Effluent Particles by Image Analysis. *Sep. Sci. Technol.* **2008**, *43*, 1737–1753. [[CrossRef](#)]
37. Li, D.; Sharp, J.O.; Saikaly, P.E.; Ali, S.; Alidina, M.; Alarawi, M.S.; Keller, S.; Hoppe-Jones, C.; Drewes, J.E. Dissolved organic carbon influences microbial community composition and diversity in managed aquifer recharge systems. *Appl. Environ. Microbiol.* **2012**, *78*, 6819–6828. [[CrossRef](#)] [[PubMed](#)]
38. Lauderdale, C.; Chadik, P.; Kirisits, M.J.; Brown, A.J. Engineered biofiltration: Enhanced biofilter performance through nutrient and peroxide addition. *J. Am. Water Work. Assoc.* **2012**, *104*, E298–E309. [[CrossRef](#)]
39. Lakretz, A.; Elifantz, H.; Kviatkovski, I.; Eshel, G.; Mamane, H. Automatic microfiber filtration (AMF) of surface water: Impact on water quality and biofouling evolution. *Water Res.* **2014**, *48*, 592–604. [[CrossRef](#)]
40. Li, H.; Durbin, R. Fast and accurate short read alignment with Burrows-Wheeler transform. *Bioinformatics* **2009**, *25*, 1754–1760. [[CrossRef](#)]
41. Shon, H.K.; Vigneswaran, S.; Snyder, S.A. Effluent Organic Matter (EfOM) in Wastewater: Constituents, Effects, and Treatment. *Crit. Rev. Environ. Sci. Technol.* **2006**, *36*, 327–374. [[CrossRef](#)]
42. Petala, M.; Tsiridis, V.; Samaras, P.; Zouboulis, A.; Sakellaropoulos, G.P. Wastewater reclamation by advanced treatment of secondary effluents. *Desalination* **2006**, *195*, 109–118. [[CrossRef](#)]
43. Grady, C.P.L.; Daigger, G.T.; Love, N.G.; Filipe, C.D.M. *Biological Wastewater Treatment*; IWA Publishing—Co-Publication: London, UK, 2011; ISBN 9781843393429.
44. Friedman, L.; Mamane, H.; Avisar, D.; Chandran, K. The role of influent organic carbon-to-nitrogen (COD/N) ratio in removal rates and shaping microbial ecology in soil aquifer treatment (SAT). *Water Res.* **2018**, *146*, 197–205. [[CrossRef](#)]
45. Cua, L.S.; Stein, L.Y. Effects of nitrite on ammonia-oxidizing activity and gene regulation in three ammonia-oxidizing bacteria. *FEMS Microbiol. Lett.* **2011**, *319*, 169–175. [[CrossRef](#)]
46. Chen, J.; Strous, M. Denitrification and aerobic respiration, hybrid electron transport chains and co-evolution. *Biochim. Biophys. Acta Bioenerg.* **2013**, *1827*, 136–144. [[CrossRef](#)] [[PubMed](#)]
47. Daims, H.; Lückner, S.; Wagner, M. A New Perspective on Microbes Formerly Known as Nitrite-Oxidizing Bacteria. *Trends Microbiol.* **2016**, *24*, 699–712. [[CrossRef](#)] [[PubMed](#)]
48. Kits, K.D.; Sedlacek, C.J.; Lebedeva, E.V.; Han, P.; Bulaev, A.; Pjevac, P.; Daebeler, A.; Romano, S.; Albertsen, M.; Stein, L.Y.; et al. Kinetic analysis of a complete nitrifier reveals an oligotrophic lifestyle. *Nature* **2017**, *549*, 269–272. [[CrossRef](#)] [[PubMed](#)]
49. Jetten, M.S.M. New pathways for ammonia conversion in soil and aquatic systems. *Plant Soil* **2001**, *230*, 9–19. [[CrossRef](#)]
50. Stein, L.Y. Heterotrophic nitrification and nitrifier denitrification. In *Nitrification*; American Society of Microbiology: Washington, DC, USA, 2011.
51. Ge, S.; Wang, S.; Yang, X.; Qiu, S.; Li, B.; Peng, Y. Detection of nitrifiers and evaluation of partial nitrification for wastewater treatment: A review. *Chemosphere* **2015**, *140*, 85–98. [[CrossRef](#)] [[PubMed](#)]
52. Park, M.R.; Park, H.; Chandran, K. Molecular and kinetic characterization of planktonic *Nitrospira* spp. selectively enriched from activated sludge. *Environ. Sci. Technol.* **2017**, *51*, 2720–2728. [[CrossRef](#)] [[PubMed](#)]
53. Siahrostami, S.; Verdaguer-Casadevall, A.; Karamad, M.; Deiana, D.; Malacrida, P.; Wickman, B.; Escudero-Escribano, M.; Paoli, E.A.; Frydendal, R.; Hansen, T.W.; et al. Enabling direct H₂O₂ production through rational electrocatalyst design. *Nat. Mater.* **2013**, *12*, 1137–1143. [[CrossRef](#)]
54. Yang, S.; Verdaguer-casadevall, A.; Arnarson, L.; Silvioli, L.; Viktor, C.; Frydendal, R.; Rossmeisl, J.; Chorkendor, I.; Stephens, I.E.L. Toward the Decentralized Electrochemical Production of H₂O₂: A Focus on the Catalysis. *ACS Catal.* **2018**, *8*, 4064–4081. [[CrossRef](#)]
55. Martin, M. Cutadapt removes adapter sequences from high-throughput sequencing reads. *EMBnet. J.* **2011**, *17*, 10–12. [[CrossRef](#)]
56. Peng, Y.; Leung, H.C.M.; Yiu, S.M.; Chin, F.Y.L. IDBA-UD: A de novo assembler for single-cell and metagenomic sequencing data with highly uneven depth. *Bioinformatics* **2012**, *28*, 1420–1428. [[CrossRef](#)]
57. Hyatt, D.; Chen, G.-L.; LoCascio, P.F.; Land, M.L.; Larimer, F.W.; Hauser, L.J. Prodigal: Prokaryotic gene recognition and translation initiation site identification. *BMC Bioinform.* **2010**, *11*, 119. [[CrossRef](#)] [[PubMed](#)]
58. Edgar, R.C. Search and clustering orders of magnitude faster than BLAST. *Bioinformatics* **2010**, *26*, 2460–2461. [[CrossRef](#)]

59. Li, H.; Durbin, R. Fast and accurate long-read alignment with Burrows-Wheeler transform. *Bioinformatics* **2010**, *26*, 589–595. [[CrossRef](#)] [[PubMed](#)]
60. Hong, C.; Manimaran, S.; Shen, Y.; Perez-Rogers, J.F.; Byrd, A.L.; Castro-Nallar, E.; Crandall, K.A.; Johnson, W.E. PathoScope 2.0: A complete computational framework for strain identification in environmental or clinical sequencing samples. *Microbiome* **2014**, *2*, 33. [[CrossRef](#)] [[PubMed](#)]



© 2020 by the authors. Licensee MDPI, Basel, Switzerland. This article is an open access article distributed under the terms and conditions of the Creative Commons Attribution (CC BY) license (<http://creativecommons.org/licenses/by/4.0/>).